

# Probing new physics at the LHC with $b\tau\nu$ final states

Andrés Florez<sup>✉\*</sup>

*Universidad de Los Andes, Carrera 1, No. 18a-12, Bogotá, Colombia*

Tomas Atehortua Garces<sup>†</sup> and José D. Ruiz-Álvarez<sup>‡</sup>

*Instituto de Física, Universidad de Antioquia, A.A. 1226, Medellín, Colombia*



(Received 17 November 2022; accepted 27 March 2023; published 13 April 2023)

The  $R_{D^{(*)}}$  anomaly is one of the most intriguing experimental results in particle physics today. Experiments such as *BABAR*, Belle and LHCb have measured a consistent tension with the Standard Model (SM). We study several extensions of the SM that could potentially explain this tension, such as production of heavy  $W'$  bosons, under the sequential SM scenario, leptoquarks with preferential couplings to third-generation fermions, and interpretations through effective field theories. Such models are not only able to explain the  $R_{D^{(*)}}$  anomaly, but also to produce distinctive signatures at the LHC. We present different feasibility studies to probe each of these scenarios at the LHC, considering final states with one b-quark candidate, one hadronically decaying tau lepton ( $\tau_h$ ) and missing transverse momentum ( $p_T^{\text{miss}}$ ). The selection criteria have been optimized for each model to achieve best signal significance. The studies are performed considering different LHC running conditions, at  $\sqrt{s} = 13$  and 13.6 TeV, and different luminosities (150 and 3000 fb<sup>-1</sup>).

DOI: [10.1103/PhysRevD.107.075010](https://doi.org/10.1103/PhysRevD.107.075010)

## I. INTRODUCTION

The Standard Model (SM) of particle physics synthesizes our understanding of fundamental particles and their interactions. Although it has been a successful theory to explain a broad set of experimental results, it does not provide answers to several questions raised at the theoretical and experimental level. With the aim to elucidate some of these conundrums, the LHC has a broad physics program to search for new particles that could explain some of the insufficiencies of the SM. A plethora of new models have been proposed, suggesting the existence of new particles such as heavy gauge bosons, neutral ( $Z'$ ) or electrically charged ( $W'$ ) [1,2], leptoquarks (LQs) [3], heavy neutrinos [4–6], new partners of the Higgs boson [7–9], and others. Many of these new ideas have been experimentally probed by the ATLAS [10] and CMS [11] experiments at the LHC, without positive results until now.

Experimental searches have used a variety of models as benchmark scenarios to set upper limits on the production cross section of the hypothetical particles, at

95% Confidence Level (CL), for a broad range of masses and couplings. For example, several searches for  $Z'$  [12–14] and  $W'$  [15–17] gauge bosons have set their exclusion ranges considering scenarios where these particles have the same couplings as those of the SM  $Z$  and  $W$  bosons. This particular benchmark model is known as the sequential SM (SSM). Existing limits to third-generation fermions are less constrained in SSM interpretations and remain important to test lepton flavor universality. In the case of LQs, the searches have been performed considering scenarios where these particles have the same couplings to all SM fermions (democratic couplings) or enhanced couplings to second- or third-generation fermions [18].

Although we currently do not have conclusive experimental evidence of physics beyond the SM, there is a set of tensions on the decay ratios of B mesons,  $R_{D^{(*)}}^{\tau/\ell'}$  ( $\ell' = e, \mu$ ) and  $R_D^{\tau/\ell'}$ , measured by the *BABAR* [19,20], Belle [21–25], and LHCb [26,27] Collaborations. To explain these experimental observations, some theoretical models and phenomenological studies propose scenarios where new particles have nonuniversal or preferential couplings to third-generation fermions [28–32].

We perform a feasibility study to assess the long-term discovery potential for resonant production of  $W'$  bosons and LQs at the LHC, considering preferential couplings to third-generation fermions, motivated by the B meson anomalies. We also consider a scenario where these hypothetical mediators are so heavy they can only be produced in off-shell processes. This approach scenario is studied with an

\*ca.florez@uniandes.edu.co

†tomas.atehortua@udea.edu.co

‡josed.ruiz@udea.edu.co

Published by the American Physical Society under the terms of the [Creative Commons Attribution 4.0 International license](https://creativecommons.org/licenses/by/4.0/). Further distribution of this work must maintain attribution to the author(s) and the published article's title, journal citation, and DOI. Funded by SCOAP<sup>3</sup>.

effective field theory (EFT) formulation. Following [33], we explore the production of  $W'$  bosons that couple to bottom (b) and charm (c) quarks on the color sector but have democratic couplings to SM leptons (SSM):  $pp \rightarrow W' + b/c$ . We consider final states where the  $W'$  decays to a tau lepton, which subsequently decays via hadronic modes ( $\tau_h$ ) and associated neutrinos ( $W' \rightarrow \tau\nu_\tau \rightarrow \tau_h\nu_\tau\nu_\tau$ ). In addition, we also explore single production of LQs, decaying to a  $\tau$  lepton ( $\tau_h$ ) and a b quark ( $LQ \rightarrow \tau b \rightarrow \tau_h\nu_\tau b$ ). Therefore, our final state is composed of a  $\tau_h$ , a b-quark jet and missing transverse momentum ( $p_T^{\text{miss}}$ ) from associated neutrino(s). The  $p_T^{\text{miss}}$  variable is defined as the magnitude of the negative vectorial sum of all reconstructed objects by the detector. This quantity is an indirect measurement of the momentum of particles that escape detection, such as neutrinos. The EFT formulation considers an effective coupling between the b and c quarks, the  $\tau$  and  $\nu_\tau$ . Although we target the same final state (b-quark,  $\tau_h$ ,  $p_T^{\text{miss}}$ ), the topology and observables vary depending on the model. For example, the b quark in the LQ scenario is significantly more energetic with respect to the same object in the  $W' + b/c$  interpretation. This affects the expected experimental sensitivity in each case.

Some similar studies have been performed in the past. In the work [34] the authors examine the final state where  $W' \rightarrow \tau\nu_\tau \rightarrow l\nu_\tau\nu_\tau$  with  $l$  being one of the light leptons of the SM. Additionally, in the work [28] the hadronic tau final state is studied; however, they only consider a  $W'$  case and develop less constraining selection criteria. In our proposal, we develop more targeted selection criteria for each new physics model case, which leads necessarily to a better discrimination power.

The studies performed within different models are carried out considering proton-proton (pp) collisions at  $\sqrt{s} = 13$  and 13.6 TeV. Different LHC luminosity scenarios are assumed. The estimation of the experimental sensitivity for each benchmark scenario is performed for different sets of masses and couplings. We determine the relevant variables and optimal thresholds to maximize experimental sensitivity.

## II. THEORETICAL MODELS

In the SSM, an additional  $SU(2)'$  symmetry group is proposed, which leads to three additional gauge bosons, one neutral,  $Z'$ , and two electrically charged  $W'^{\pm}$  [35]. Depending on the realization of the model, different couplings to leptons are considered. The Lagrangian for the charged current is defined in Eq. (1), where CC stands for charged current and the  $g_2'$  factor is the coupling constant for the additional  $SU(2)'$  group. The  $\kappa$  parameters are complex values of  $3 \times 3$  matrices in the flavor space.

$$\begin{aligned} \mathcal{L}_{\text{CC}}^{W'} = & \frac{g_2'}{\sqrt{2}} \bar{u}_i \gamma^\mu ([\kappa_{q,L}^{W'}]_{ij} P_L + [\kappa_{q,R}^{W'}]_{ij} P_R) d_j \\ & + \frac{g_2'}{\sqrt{2}} \bar{\nu}_i \gamma^\mu ([\kappa_{\ell,L}^{W'}]_{ij} P_L + [\kappa_{\ell,R}^{W'}]_{ij} P_R) \ell_j W'_\mu + \text{H.c.} \quad (1) \end{aligned}$$

In Eq. (1) the  $P_{R,L}$  are the chiral projectors. The structure of the Lagrangian is similar to that of the SM, and in fact the SM can be recovered by performing the replacements outlined in Eq. (2) below and summing over quark and lepton flavors, as described in [36]. In the same equation  $V_{ij}^{\text{CKM}}$  are the Cabibbo-Kobayashi-Maskawa (CKM) matrix elements and the  $V_{ij}^{\text{PMNS}}$  are the lepton mixing matrix elements. In this model, the  $W'$  and the  $Z'$  masses are free parameters. For the purpose of our final state, we consider the case where the  $W'$  has preferential couplings to the third-generation leptons. However, for this work we consider, as in [37], a ‘‘simplified phenomenological approach’’ where the  $\kappa$  parameters are free. The new neutral current does not provide any contributions to the final state we consider in this work.

$$\begin{aligned} [\kappa_{q,L}^{W'}]_{ij} &= V_{ij}^{\text{CKM}}, & [\kappa_{\ell,L}^{W'}]_{ij} &= V_{ij}^{\text{PMNS}}, & \kappa_{q(\ell),R}^{W'} &= 0, \\ [\kappa_{f,L}^{Z'}]_{ij} &= (T_L^{3,f} - Q_f \sin^2 \theta_W) \delta_{ij}, \\ [\kappa_{f,R}^{Z'}]_{ij} &= (-Q_f \sin^2 \theta_W) \delta_{ij}. \end{aligned} \quad (2)$$

In addition to the  $W'/Z'$  model described above, we consider models with LQs as massive intermediate particles, with fractional electric charge, that couple simultaneously to leptons and quarks [3]. These hypothetical particles could be of scalar or vectorial nature, depending on the model, and their mass is a free parameter. As an example, Eq. (3) shows the Lagrangian for a vectorial LQ defined as  $U_1$ , with quantum numbers  $(3_C, 1_I, 2/3_Y)$ , that couples to the second and third families of quarks and leptons. In the same equation,  $l_{2,3}$  and  $q_{2,3}$  refer to the SM fermion doublets.

$$\begin{aligned} \mathcal{L}_U \supset & U_{1,\mu} (\lambda_{33} \bar{q}_3 \gamma^\mu P_L l_3 + \lambda_{32} \bar{q}_3 \gamma^\mu P_L l_2 \\ & + \lambda_{23} \bar{q}_2 \gamma^\mu P_L l_3 + \lambda_{22} \bar{q}_2 \gamma^\mu P_L l_2) + \text{H.c.} \quad (3) \end{aligned}$$

For our final model, we consider an EFT formulation. An EFT is an approximation that allows us to include degrees of freedom to describe phenomena occurring at a certain energy scale, without considering the substructure of the interactions at higher energies or other underlying physics phenomena [38]. An EFT only includes relevant degrees of freedom, i.e., those states with  $m \ll \Lambda$  while heavier excitations with  $M \gg \Lambda$  are integrated out from the action [39–43].  $\Lambda$  is the cutoff scale which defines the energy scale for the new physics. This means that the heavier degrees of freedom for new physics appear in the ‘‘low-energy Lagrangian’’ as effective terms. The representative Lagrangian for the EFT model considered in these studies is shown in Eq. (4):

$$\begin{aligned} \mathcal{L}_{\text{eff}} \supset & -\frac{2V_{ib}}{v^2} [(1 + \epsilon_L^{ib})(\bar{\tau} \gamma_\mu P_L \nu_\tau)(\bar{u}_i \gamma^\mu P_L b) \\ & + \epsilon_R^{ib}(\bar{\tau} \gamma_\mu P_L \nu_\tau)(\bar{u}_i \gamma^\mu P_R b) \\ & + \epsilon_T^{ib}(\bar{\tau} \sigma_{\mu\nu} P_L \nu_\tau)(\bar{u}_i \sigma^{\mu\nu} P_L b) \\ & + \epsilon_{S_L}^{ib}(\bar{\tau} P_L \nu_\tau)(\bar{u}_i P_L b)] + \text{H.c.} \quad (4) \end{aligned}$$

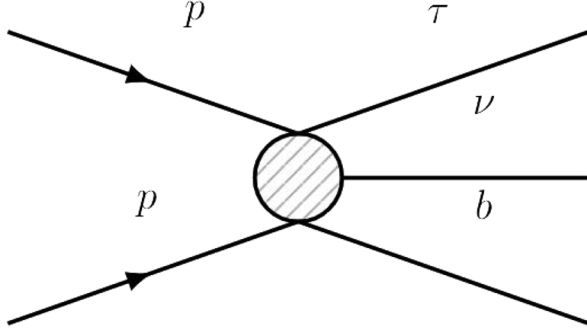


FIG. 1. Feynman diagram of  $pp \rightarrow b\tau\nu$  production for the EFT model. The circle in the middle represents the new physics that could explain the  $R_{D^*}$  anomaly. We do not specify the nature of the final state particles as particles or their antiparticles, as we are interested in all the possible final states.

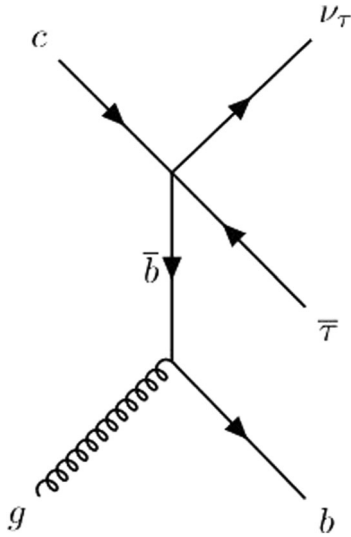


FIG. 2. Representative Feynman diagram for the EFT model, that could lead to the final state of interest, that could explain the  $R_{D^*}$  anomaly.

In Eq. (4),  $V_{ij}$  are the CKM matrix elements,  $\sigma^{\mu\nu} = (i/2)[\gamma^\mu, \gamma^\nu]$ ,  $v \approx 246$  GeV is the electroweak symmetry breaking scale, and  $\epsilon_\tau$  are the Wilson coefficients [44]. Figures 1 and 2 show representative Feynman diagrams for the EFT interpretation.

### III. SIMULATED SAMPLES

Signal and background samples are generated at parton level using `MadGraph5_aMC` (v2.6.3.2) [45], considering  $pp$  collisions with a center-of-mass energy of  $\sqrt{s} = 13$  and 13.6 TeV. For the parton distribution function (PDF), the NNPDF3.0 NLO [46] set is used in the event generation of all simulated samples. At this stage, jets are required to have a minimum transverse momentum ( $p_T$ ) of 30 GeV and  $|\eta| < 5.0$ . Generated partonic events are then passed through the `PYTHIA 8` (v8.2.05) [47] package to include

hadronic processes. The `DELPHES` (v3.4.1) [48] software is used to emulate detector response, using the CMS detector configuration, for particle reconstruction and identification efficiencies.

The MLM algorithm [49,50] is used for jet matching and jet merging. This process is used for the simulation of backgrounds which include additional jets. We follow the common recommendations for this procedure.

The dominant sources of background events come from the production of a SM Z (W) gauge boson with associated jets, referred to as Z + jets (W + jets), and the production of pairs of top quarks with additional jets ( $t\bar{t}$ ). Events from single production of top quarks plus jets, gauge boson pairs (WW, ZZ, WZ), and from quantum chromodynamic interactions among light quarks (QCD multijets) are also considered but deemed negligible after applying the main event selection criteria to search for signal. Based on the final state objects used in the study,  $2 \times 10^6$  events are produced for each background, considering leptonic decays for the Z + jets (W + jets) background and semileptonic final states for  $t\bar{t}$ .

The production cross sections for all simulated processes are estimated using `MadGraph5` at leading-order precision. Table I shows the cross sections we use for the different signal models and Table II for the background samples.

Signal samples are produced as  $pp \rightarrow b\tau\nu$  without additional jets, using a `FeynRules` [51] implementation interfaced with `MadGraph` in the UFO format [52]. We use the same models utilized in [44]. For the  $W'$  model, we only consider couplings to b and c quarks,  $g_q$ , as well to  $\tau$  and  $\nu_\tau$ ,  $g_l$ . The simulated samples are produced considering  $g_q = g_l = 1.0$  and masses of 0.6, 1.0, 1.6, 2.0, 2.5, 3.0, and 3.5 TeV, with 50 000 events per sample. For the LQ case, we produce samples with  $g_{bl} = g_{cl} = 1.0$  (couplings of the LQ and the b or quark and leptons) and masses of 0.5, 1.0, 1.25, 1.5, 2.0, and 3.0 TeV, with 100 000 events per sample. For the  $W'$  and LQ samples, the corresponding decay widths are left to be automatically calculated by `MadGraph`. For the EFT scenario we consider separately the case with a scalar, vectorial, and tensor coupling. For each case we produce a Monte Carlo sample, considering a coupling of 1.0 and 100 000 events per sample.

It is important to stress that for the development of the search strategy we have considered some benchmark points for the models. These selected benchmarks are chosen on their relevance for the LHC search and not as a function of their compatibility to low-energy constraints nor their capability to explain the  $R_{D^{(*)}}$  anomaly only. The experimental search is constrained by the kinematics of the signal, which is crucial for the optimization of the selection criteria. Therefore, the most relevant characteristic for the LQ and  $W'$  models is the mediator mass. The value of the couplings and the Wilson coefficients are only important to determine the total production cross section of the signal. In this sense, we will show results for benchmark points under

TABLE I. Signal parametrization and cross sections.

Model	Parameters	Cross section 13 TeV [pb]	Cross section 13.6 TeV [pb]
SSM	$m_{W'} = 6.0 \times 10^2$ GeV	5.25	5.88
	$m_{W'} = 1.0 \times 10^3$ GeV	0.45	0.52
	$m_{W'} = 1.6 \times 10^3$ GeV	$3.04 \times 10^{-2}$	$3.45 \times 10^{-2}$
	$m_{W'} = 2.0 \times 10^3$ GeV	$1.06 \times 10^{-2}$	$1.26 \times 10^{-2}$
	$m_{W'} = 2.5 \times 10^3$ GeV	$3.11 \times 10^{-3}$	$3.58 \times 10^{-3}$
	$m_{W'} = 3.0 \times 10^3$ GeV	$1.18 \times 10^{-3}$	$1.36 \times 10^{-3}$
EFT	$\epsilon_L^{cb} = 1.0$	0.13	0.14
	$\epsilon_{S_L}^{cb} = 1.0$	$8.07 \times 10^{-2}$	$9.08 \times 10^{-2}$
	$\epsilon_T^{cb} = 1.0$	0.71	0.79
LQ-U <sub>1</sub>	$m_{LQ} = 5.0 \times 10^2$ GeV	0.74	0.93
	$m_{LQ} = 1.0 \times 10^3$ GeV	$2.44 \times 10^{-2}$	$2.94 \times 10^{-2}$
	$m_{LQ} = 1.25 \times 10^3$ GeV	$6.80 \times 10^{-2}$	$8.56 \times 10^{-3}$
	$m_{LQ} = 1.5 \times 10^3$ GeV	$2.20 \times 10^{-3}$	$2.77 \times 10^{-3}$
	$m_{LQ} = 2.0 \times 10^3$ GeV	$3 \times 10^{-4}$	$3.94 \times 10^{-4}$
	$m_{LQ} = 3.0 \times 10^3$ GeV	$9.82 \times 10^{-6}$	$1.24 \times 10^{-5}$

TABLE II. Production cross section for dominant backgrounds.

Process	Monte Carlo restrictions	Cross section 13 TeV [pb]	Cross section 13.6 TeV [pb]
$t\bar{t}$	...	504.0	558.9
W + jets	ptl = 190 GeV, miset = 160 GeV	0.64	0.71
DY + jets	ptl = 190 GeV	0.25	0.27

the LHC reach and that are not necessarily expected to be consistent with low-energy constraints.

#### IV. EVENT SELECTION CRITERIA

The event selection criteria are divided in two sets. The first set, defined as baseline selections, contains the requirements used similarly across the three different models under study. These selections allow us to define the phase space and objects to search for each type of signal. Events with one  $\tau_h$  candidate, zero electrons or muons, and exactly one b-quark jet are selected, following the studies performed in Ref. [33]. Events with two or more  $\tau_h$  candidates with  $p_T$  above 50 GeV and  $|\eta_\tau| < 2.3$  are rejected. The baseline selections are summarized in Table III. The second set of selections, presented in Table IV, is associated with the topological characteristics of each model. These selections and the corresponding thresholds have been chosen using a  $\frac{N_s}{\sqrt{N_s+N_b}}$  figure of merit, in order to obtain the best signal significance, where  $N_s$  ( $N_b$ ) represents the expected number of signal (background) events, normalized to cross section and luminosity.

#### V. RESULTS

After selecting events passing the selection criteria outlined in Tables III and IV, three different observables,

one per model, are chosen to assess the presence of signal events among the background expectation. These observables are found to give the best separation between signal and background events, maximizing the expected

TABLE III. Baseline selection criteria used for the different models under study.

Criterion	Selection
$N(\tau_h)$	$> 0$
$ \eta_\tau $	$\leq 2.3$
Veto 2 <sup>nd</sup> - $\tau_h$	$p_T > 50$ GeV and $ \eta  < 2.3$
$N_{e/\mu}$ with $p_T(e/\mu) > 15$ GeV	$= 0$
$N_{b\text{-jets}}$	$= 1$
$p_T(b)$	$> 20$ GeV
$ \eta_{b\text{-jets}} $	$< 2.5$

TABLE IV. Topological selections for the three different models, W', LQ and EFT, considered in the analysis. Thresholds have been selected based on best signal significance.

Parameter	SSM	EFT	U1 LQ
$p_T(\tau) >$	250 GeV	200 GeV	300 GeV
$ \Delta\phi(\tau, p_T^{\text{miss}})  >$	1.5	2.0	1.0
$p_T^{\text{miss}} >$	200 GeV	300 GeV	400 GeV

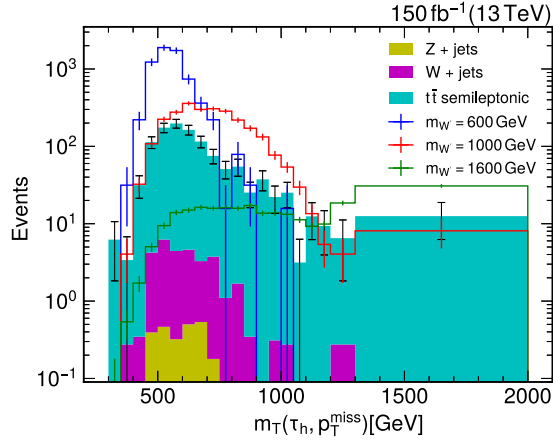


FIG. 3. Distribution of the  $m_T(\tau_h, p_T^{\text{miss}})$  variable, for the background prediction and three different signal points. The backgrounds are represented by solid colors and are stacked on top of each other, while the signal samples are represented by solid lines and overlaid on top of the background. The expected events are estimated for an integrated luminosity of  $150 \text{ fb}^{-1}$  and  $\sqrt{s} = 13 \text{ TeV}$ .

experimental sensitivity. For the  $W'$  scenario, the transverse mass between the  $\tau_h$  candidate and expected missing transverse momentum, defined as  $m_T(\tau_h, p_T^{\text{miss}}) = \sqrt{2p_T(\tau_h)p_T^{\text{miss}} \times \cos(\Delta\phi(\tau_h, p_T^{\text{miss}}))}$ , is chosen. The  $m_T(\tau_h, p_T^{\text{miss}})$  distribution is shown in Fig. 3. The figure shows the background expectation in solid format, stacked, and three different signal samples overlaid on top of the background. Events are normalized based on the cumulative efficiency after all the selections, the production cross sections, and integrated luminosity of  $150 \text{ fb}^{-1}$ . The choice of luminosity is based on the performance of the LHC during 2016–2018 for pp collisions at  $\sqrt{s} = 13 \text{ TeV}$ .

For the LQ model, the reconstructed mass between the  $\tau_h$  and b-quark candidates is used as the main observable to search for signal. Figure 4 shows the corresponding distributions, following the same conventions as those used for  $m_T(\tau_h, p_T^{\text{miss}})$ .

Since the EFT is a pointlike interaction, there is no on-shell mediator considered for these signals. In that sense, the interpretation of a peak in the histograms does not mean the same as a peak for the SSM samples. For this model, we use an observable, defined mathematically as  $m_{\text{Tot}} = \sqrt{(p_T(\tau_h) + p_T(b) + p_T^{\text{miss}})^2 - (\mathbf{p}_T(\tau_h) + \mathbf{p}_T(b) + \mathbf{p}_T^{\text{miss}})^2}$  and named as the total mass, using the  $\tau_h$ , the b-quark jet and the  $p_T^{\text{miss}}$ . The distribution for background and three signal points is shown in Fig. 5.

Table V shows the expected number of events, for three different masses, for the  $W'$  and LQ models and for three different couplings for the EFT interpretation, and for the dominant backgrounds.

To determine the discovery reach for each model and assess differences, we use a profile likelihood test statistic

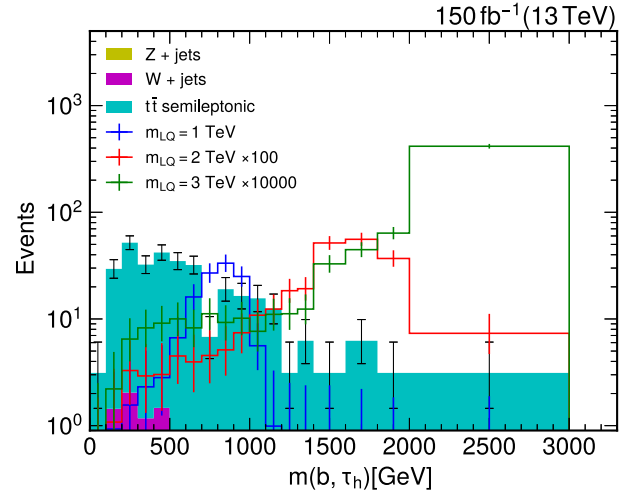


FIG. 4. Distribution of the reconstructed mass between the  $\tau_h$  and b-quark jet candidates. The backgrounds are represented by solid colors and are stacked while the signal samples are represented by solid lines and overlaid on top of the background. The expected event yields are estimated for an integrated luminosity of  $150 \text{ fb}^{-1}$  and  $\sqrt{s} = 13 \text{ TeV}$ .

using the expected number of background and signal events in each bin of the distributions shown in Figs. 3–5. We perform a maximum likelihood fit using the full range of these observables, employing a software package developed by the CERN laboratory known as ROOT-Fit [53]. Systematic uncertainties are incorporated into the calculations as nuisance parameters, considering log priors for normalization and Gaussian priors for shape uncertainties. The significance is calculated using the local  $p$  value, estimated as the probability under a null signal hypothesis

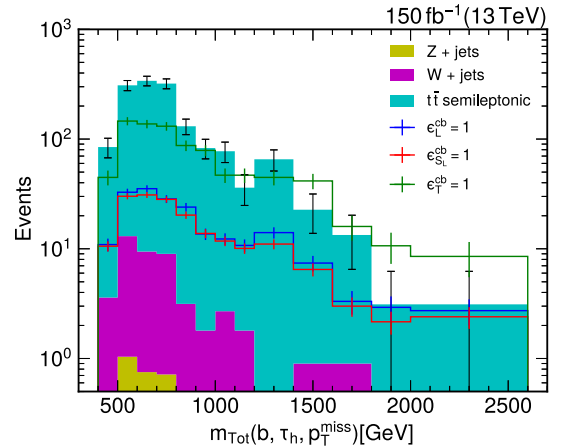


FIG. 5. Distribution of the total mass  $m_{\text{Tot}}$  for the EFT benchmark scenario. The backgrounds are represented by solid colors and are stacked, while the signal samples are represented by solid lines and overlaid on top of the background. The expected event yields are estimated for an integrated luminosity of  $150 \text{ fb}^{-1}$  and  $\sqrt{s} = 13 \text{ TeV}$ .

TABLE V. Expected number of events after the baseline and topological selection criteria, for the different signal models considered. The estimations are performed for  $\sqrt{s} = 13$  and 13.6 TeV and  $150 \text{ fb}^{-1}$  luminosity.

	$\sqrt{s} = 13 \text{ TeV}$		$\sqrt{s} = 13.6 \text{ TeV}$	
	Baseline	Topological	Baseline	Topological
		SSM $W'$		
$m_{W'} = 0.6 \text{ TeV}$	$8.55 \times 10^4$	$6.57 \times 10^3$	$9.40 \times 10^4$	$7.22 \times 10^3$
$m_{W'} = 1.0 \text{ TeV}$	$7.78 \times 10^3$	$2.46 \times 10^3$	$8.55 \times 10^3$	$2.87 \times 10^3$
$m_{W'} = 1.6 \text{ TeV}$	$5.09 \times 10^2$	$2.48 \times 10^2$	$5.60 \times 10^2$	$2.72 \times 10^2$
$m_{W'} = 2.0 \text{ TeV}$	$1.68 \times 10^2$	$8.73 \times 10^1$	$1.85 \times 10^2$	$9.63 \times 10^1$
$m_{W'} = 2.5 \text{ TeV}$	$4.60 \times 10^1$	$2.30 \times 10^1$	$5.06 \times 10^1$	$2.53 \times 10^1$
$m_{W'} = 3.0 \text{ TeV}$	$1.66 \times 10^1$	$7.25 \times 10^0$	$1.82 \times 10^1$	$7.97 \times 10^0$
$\bar{t}\bar{t}$	$1.80 \times 10^6$	$1.11 \times 10^3$	$1.98 \times 10^6$	$1.22 \times 10^3$
W + jets	$3.48 \times 10^3$	$2.86 \times 10^1$	$3.83 \times 10^3$	$3.14 \times 10^1$
Z + jets	$7.41 \times 10^1$	$2.79 \times 10^0$	$8.70 \times 10^1$	$3.06 \times 10^0$
		LQ		
$m_{LQ} = 0.6 \text{ TeV}$	$2.19 \times 10^4$	$1.52 \times 10^2$	$2.75 \times 10^4$	$1.92 \times 10^2$
$m_{LQ} = 1.0 \text{ TeV}$	$5.56 \times 10^2$	$1.24 \times 10^2$	$7.01 \times 10^2$	$1.55 \times 10^2$
$m_{LQ} = 1.25 \text{ TeV}$	$1.77 \times 10^2$	$4.98 \times 10^1$	$2.23 \times 10^2$	$6.22 \times 10^1$
$m_{LQ} = 1.5 \text{ TeV}$	$5.42 \times 10^1$	$1.79 \times 10^1$	$6.84 \times 10^1$	$2.25 \times 10^1$
$m_{LQ} = 2.0 \text{ TeV}$	$6.71 \times 10^0$	$2.48 \times 10^0$	$8.47 \times 10^0$	$3.13 \times 10^0$
$m_{LQ} = 3.0 \text{ TeV}$	$1.82 \times 10^{-1}$	$6.86 \times 10^{-2}$	$2.29 \times 10^{-1}$	$8.64 \times 10^{-2}$
$\bar{t}\bar{t}$	$1.80 \times 10^6$	$3.11 \times 10^2$	$1.98 \times 10^6$	$3.42 \times 10^2$
W + jets	$3.48 \times 10^3$	$8.80 \times 10^0$	$3.83 \times 10^3$	$9.82 \times 10^0$
Z + jets	$7.41 \times 10^1$	$7.16 \times 10^{-1}$	$8.70 \times 10^1$	$7.87 \times 10^{-1}$
		EFT		
EFT $\epsilon_L^{cb} = 1$	$1.52 \times 10^3$	$1.94 \times 10^2$	$1.71 \times 10^3$	$2.18 \times 10^2$
EFT $\epsilon_S^{cb} = 1$	$9.09 \times 10^2$	$1.81 \times 10^2$	$9.99 \times 10^2$	$1.99 \times 10^2$
EFT $\epsilon_T^{cb} = 1$	$1.09 \times 10^4$	$8.41 \times 10^2$	$1.31 \times 10^4$	$1.01 \times 10^3$
$\bar{t}\bar{t}$	$1.80 \times 10^6$	$1.45 \times 10^3$	$1.98 \times 10^6$	$1.59 \times 10^3$
W + jets	$3.48 \times 10^3$	$4.26 \times 10^1$	$3.83 \times 10^3$	$4.68 \times 10^1$
Z + jets	$7.41 \times 10^1$	$3.69 \times 10^0$	$8.70 \times 10^1$	$4.05 \times 10^0$

to obtain a value of the test statistic as large as that obtained with a signal plus background hypothesis. Similar to Refs. [54–59], the signal significance  $\sigma_{\text{sig}}$  is obtained by calculating the value at which the integral of a Gaussian between  $\sigma_{\text{sig}}$  and  $\infty$  matches the local  $p$  value. We consider a 3% systematic uncertainty associated with the measurement of the integrated luminosity at the LHC, 5% due to the PDF set used for the production of the simulated events for signal and MC, following the PDF4LHC prescription [60], 5% on the identification of  $\tau_h$  candidates and 5% on the associated measurement of their energy scale, 3% on b-quark jet [61] identification efficiencies and a flat 10% uncertainty to account for other sources of experimental effects, such as the resolution on the  $p_T^{\text{miss}}$  estimation.

Figure 6 shows the expected signal significance for the  $W'$  (LQ) model as a function of mass, for an integrated luminosity of  $150 \text{ fb}^{-1}$ . For the SSM  $W'$  (LQ) model, masses up to 2900 GeV (1600 GeV) can be excluded considering  $1.69\sigma$  of signal significance, while masses up to 2300 GeV (1200 GeV) could potentially be discovered with  $5\sigma$  signal significance above the background

expectation. In addition, for the high-luminosity LHC (HLLHC) at  $\sqrt{s} = 13.6 \text{ TeV}$  and  $3000 \text{ fb}^{-1}$  luminosity, the projections show the extension of the exclusion reach to masses beyond 3 TeV for the SSM  $W'$  scenario, as shown in Fig. 7. In the case of single LQ production, it is feasible to probe masses up to 2100 GeV, while the sensitivity for discovery at  $5\sigma$  goes up to 1800 GeV. Table VI shows the corresponding results for the EFT interpretation, for the three different coupling scenarios and LHC operation and luminosity conditions that have been considered.

In addition, Fig. 8 shows a comparison among the preferred phase space on LQ and  $W'$  model for the  $R_{D^{(*)}}$  anomaly and the exclusions we have found from our search proposal. To make this comparison, we have set the  $W'$  coupling to leptons to 1 while varying the coupling to quarks. This directly impacts the production cross section for the mediator. For the LQ case, we have set  $g_{cl} = 1$  and have varied  $g_{bl}$ . The exclusion lines denote the exclusion achieved for  $1.69\sigma$  from our proposal. Therefore, the area with a greater coupling strength from these lines is excluded. We can see from this comparison that we are

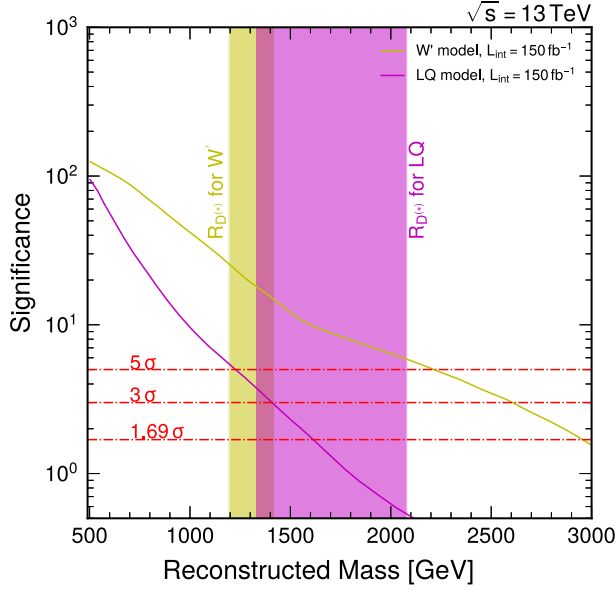


FIG. 6. Expected signal significance for the  $W'$  and LQ benchmark scenarios, as a function of the corresponding reconstructed mass, considering an integrated luminosity of  $150 \text{ fb}^{-1}$  and  $\sqrt{s} = 13 \text{ TeV}$ . We also show the 1-sigma bands that explain  $R_{D^{(*)}}$  as in [44] and in [62], setting the corresponding couplings to 1.

able to exclude all the area preferred by the  $R_{D^{(*)}}$  anomaly for the  $W'$  model. However, some phase space for the LQ model remains without exclusion.

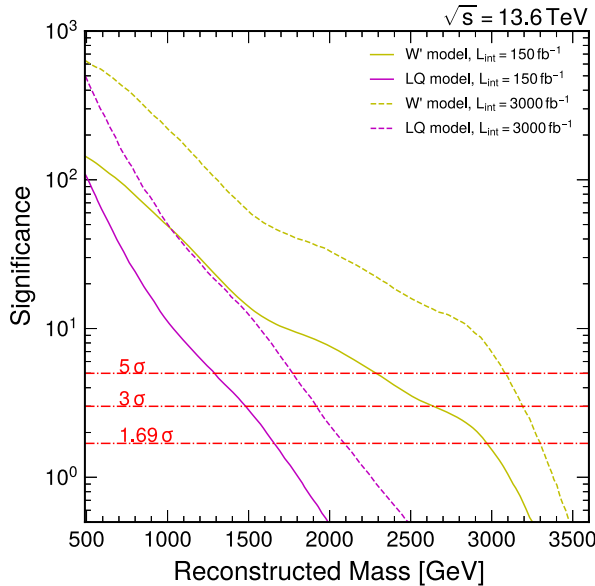


FIG. 7. Expected signal significance for the  $W'$  and LQ benchmark scenarios, as function of the corresponding reconstructed mass, considering an integrated luminosity of  $150 \text{ fb}^{-1}$  for  $\sqrt{s} = 13 \text{ TeV}$  and  $\sqrt{s} = 13.6 \text{ TeV}$  and  $3000 \text{ fb}^{-1}$  for  $\sqrt{s} = 13.6 \text{ TeV}$ .

TABLE VI. Signal significance for the EFT benchmark scenario, considering integrated luminosities of  $150 \text{ fb}^{-1}$  for  $\sqrt{s} = 13 \text{ TeV}$  and  $\sqrt{s} = 13.6 \text{ TeV}$  and  $3000 \text{ fb}^{-1}$  for  $\sqrt{s} = 13.6 \text{ TeV}$ .

EFT	$\sqrt{s} = 13 \text{ TeV}$ ( $L_{\text{int}} = 150 \text{ fb}^{-1}$ )	$\sqrt{s} = 13.6 \text{ TeV}$ ( $L_{\text{int}} = 150 \text{ fb}^{-1}$ )	$\sqrt{s} = 13.6 \text{ TeV}$ ( $L_{\text{int}} = 3000 \text{ fb}^{-1}$ )
$\epsilon_{S_L}^{cb}$	2.3	2.4	10.6
$\epsilon_L^{cb}$	2.7	2.8	12.4
$\epsilon_T^{cb}$	9.2	10.2	45.4

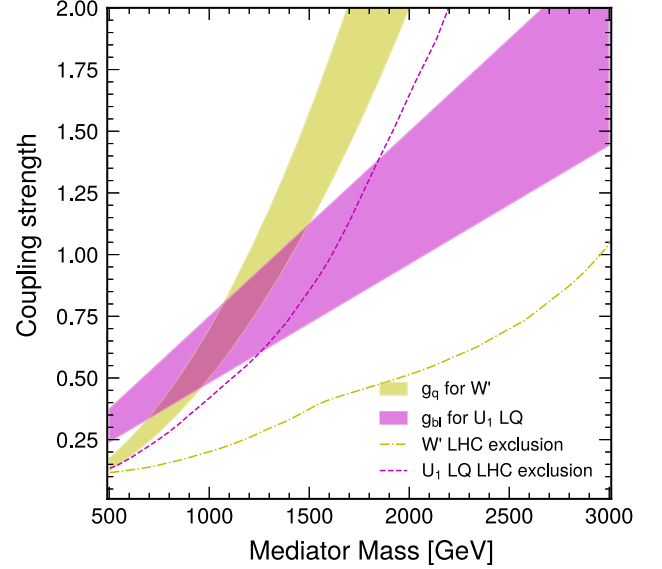


FIG. 8. Preferred bands, in solid color, for the  $R_{D^{(*)}}$  anomaly compared to the LHC expected exclusion, in dotted lines for the LQ and  $W'$  models. The exclusion lines mark the lowest coupling strength reachable by our search with  $150 \text{ fb}^{-1}$  at  $\sqrt{s} = 13 \text{ TeV}$ .

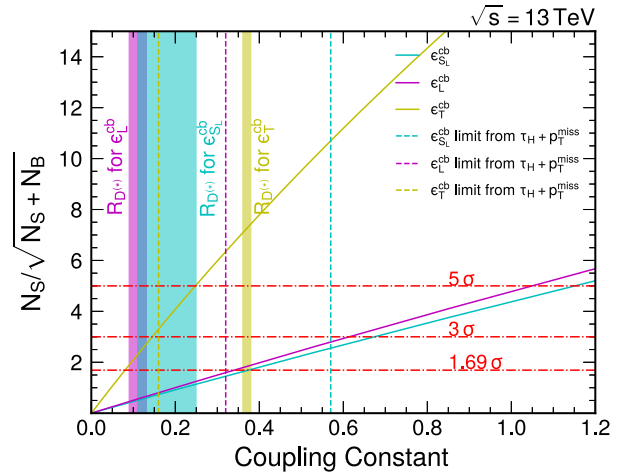


FIG. 9. Expected signal significance for the EFT benchmark scenarios, as function of the corresponding strength of the interaction, considering an integrated luminosity of  $150 \text{ fb}^{-1}$  for  $\sqrt{s} = 13 \text{ TeV}$ . The 1-sigma bands explain the  $R_{D^{(*)}}$  anomaly as in [44], while the vertical dashed lines show the limits derived in [44], using a  $\tau_h + p_T^{\text{miss}}$  final state.

TABLE VII. Expected experimental sensitivity to probe the Wilson coefficients considered in the EFT interpretation, for different LHC conditions.

Data	$Z = 1.69\sigma$			$Z = 3\sigma$			$Z = 5\sigma$		
	Run 2	Run 3	HLLHC	Run 2	Run 3	HLLHC	Run 2	Run 3	HLLHC
$c_{S_L}^{cb}$	0.37	0.34	0.07	0.67	0.61	0.14	1.15	1.05	0.25
$c_{L}^{cb}$	0.34	0.31	0.06	0.61	0.56	0.13	1.05	0.95	0.21
$c_T^{cb}$	0.08	0.07	0.01	0.14	0.12	0.03	0.25	0.21	0.05

## VI. DISCUSSION AND CONCLUSIONS

Our findings have been interpreted in various models and therefore we have to discuss the implications in each of the scenarios. Firstly, while the current searches for a  $W'$  at the LHC, for the  $\tau + p_T^{\text{miss}}$  final state quote exclusion limits up to 4.6 TeV [63,64] in the mass of the  $W'$ , our proposal covers a new signature which must exist if a  $W'$  is the responsible for the anomalies on the B meson decay ratios. In this sense, our proposal pinpoints the specific physics process which would be a consequence of the observed B meson anomalies, while the generic searches for a  $W'$  cover a broader spectrum of processes. It is important to mention that the inclusion of a b-quark jet in the final state changes significantly the expected amount and composition of the background, with respect to the inclusive search.

In addition, the signature considered in this work is a novel signature to search for LQs. The closest final state considered in the literature for LQ searches studies final states with two  $\tau_h$  and one b-jet candidates. The exclusion limit achieved by that search sets a limit on the LQ mass, which should be greater than 1.1 TeV [65]. Therefore, our proposal reaches a higher and more stringent limit for the LQ mass and also explores a new channel relevant to study B meson anomalies. The gain in experimental sensitivity is associated with more optimal selection criteria, specially when considering only one  $\tau_h$  candidate instead of two. The identification efficiency for  $\tau_h$  candidates is not very high, on average 60%.

For the EFT interpretation, we also reach new and complementary results with regard to the state of the art. In Fig. 9 is shown the comparison among the limits

achieved by our proposal and the limits derived in [44]. We can see that the limits using  $b + \tau_h + p_T^{\text{miss}}$  signature are competitive with the  $\tau_h + p_T^{\text{miss}}$  results. Additionally, from the physics point of view, both final states should exist if the assumed couplings exist and, therefore, our proposal makes a direct test of the underlying physics. In Table VII are displayed the sensitivities, defined as  $N_S/\sqrt{N_S + N_B}$ , that can be achieved for each EFT interpretation at the current operation energies for the LHC.

Finally, we have developed a completely new strategy to address three different scenarios in a common final state taking into account the particularities of each model. In this sense, we have proposed a strategy that would be able to include information on the characteristics of a hypothetical signal in the LHC depending on the observable. In other words, we have shown how a signal in the considered final state does not have the same features for the possible theoretical models giving rise to it.

## ACKNOWLEDGMENTS

We wish to acknowledge the support of Ocampo-Henao who helped us with technical analysis tools. J. D. R.-A. and T. A. G. gratefully acknowledge the support of the Colombian Science Ministry MinCiencias with the grant Minciencias CD 82315 CT ICETEX 2021-1080 and Sostenibilidad-UdeA. A. F. thanks the constant and enduring financial support received for this project from the faculty of science at Universidad de Los Andes (Bogotá, Colombia) and the Colombian Science Ministry MinCiencias, with Grant Program No. 70141.

- 
- [1] P. K. Mohapatra, R. N. Mohapatra, and P. B. Pal, Implications of E6 grand unification, *Phys. Rev. D* **33**, 2010 (1986).
  - [2] Joseph D. Lykken, Z-prime bosons and supersymmetry, eConf **C960625**, NEW140 (1996).
  - [3] Martin Schmaltz and Yi-Ming Zhong, The leptoquark Hunter's guide: Large coupling, *J. High Energy Phys.* **01** (2019) 132.
  - [4] Janusz Gluza and Tomasz Jelinski, Heavy neutrinos and the  $pp \rightarrow lljj$  CMS data, *Phys. Lett. B* **748**, 125 (2015).
  - [5] P. Astier, D. Autiero, A. Baldisseri, M. Baldo-Ceolin, M. Banner, G. Bassompierre, K. Benslama, N. Besson, I. Bird, B. Blumenfeld *et al.*, Search for heavy neutrinos mixing with tau neutrinos, *Phys. Lett. B* **506**, 27 (2001).
  - [6] G. Aad, B. Abbott, J. Abdallah, S. Abdel Khalek, R. Aben, B. Abi, M. Abolins, O. S. AbouZeid, H. Abramowicz,

- H. Abreu *et al.*, Search for heavy Majorana neutrinos with the atlas detector in  $pp$  collisions at  $\sqrt{s} = 8$  TeV, *J. High Energy Phys.* **07** (2015) 162.
- [7] Adam Falkowski, Christian Gross, and Oleg Lebedev, A second Higgs from the Higgs portal, *J. High Energy Phys.* **05** (2015) 057.
- [8] Alejandro Celis, Victor Ilisie, and Antonio Pich, LHC constraints on two-Higgs doublet models, *J. High Energy Phys.* **07** (2013) 053.
- [9] Arsham Farzinnia and Jing Ren, Higgs partner searches and dark matter phenomenology in a classically scale invariant Higgs boson sector, *Phys. Rev. D* **90**, 015019 (2014).
- [10] G. Aad *et al.*, The ATLAS experiment at the CERN large hadron collider, *J. Instrum.* **3**, S08003 (2008).
- [11] S. Chatrchyan *et al.*, The CMS experiment at the CERN LHC, *J. Instrum.* **3**, S08004 (2008).
- [12] A. M. Sirunyan *et al.*, Search for resonant and nonresonant new phenomena in high-mass dilepton final states at  $\sqrt{s} = 13$  TeV, *J. High Energy Phys.* **07** (2021) 208.
- [13] G. Aad *et al.*, Search for high-mass dilepton resonances using  $139 \text{ fb}^{-1}$  of  $pp$  collision data collected at  $\sqrt{s} = 13$  TeV with the ATLAS detector, *Phys. Lett. B* **796**, 68 (2019).
- [14] CMS Collaboration *et al.*, Search for heavy narrow dilepton resonances in  $pp$  collisions at  $\sqrt{s} = 7$  TeV and  $\sqrt{s} = 8$  TeV, *Phys. Lett. B* **720**, 63 (2013).
- [15] CMS Collaboration *et al.*, Search for  $w'$  decaying to tau lepton and neutrino in proton-proton collisions at  $\sqrt{s} = 8$  TeV, *Phys. Lett. B* **755**, 196 (2016).
- [16] CMS Collaboration *et al.*, Search for a  $w'$  boson decaying to a  $\tau$  lepton and a neutrino in proton-proton collisions at  $\sqrt{s} = 13$  TeV, *Phys. Lett. B* **792**, 107 (2019).
- [17] ATLAS Collaboration *et al.*, Search for a heavy gauge boson decaying to a charged lepton and a neutrino in  $1 \text{ fb}^{-1}$  of  $pp$  collisions at  $\sqrt{s} = 7$  TeV using the ATLAS detector, *Phys. Lett. B* **705**, 28 (2011).
- [18] A. M. Sirunyan *et al.*, Search for singly and pair-produced leptoquarks coupling to third-generation fermions in proton-proton collisions at  $s = 13$  TeV, *Phys. Lett. B* **819**, 136446 (2021).
- [19] BABAR Collaboration, Measurement of an excess of  $\bar{B} \rightarrow D^{(*)}\tau^{-}\bar{\nu}_{\tau}$  decays and implications for charged Higgs bosons, *Phys. Rev. D* **88**, 072012 (2013).
- [20] BABAR Collaboration, Evidence for an Excess of  $\bar{B} \rightarrow D^{(*)}\tau^{-}\bar{\nu}_{\tau}$  Decays, *Phys. Rev. Lett.* **109**, 101802 (2012).
- [21] G. Caria *et al.* (Belle Collaboration), Measurement of  $\mathcal{R}(D)$  and  $\mathcal{R}(D^*)$  with a semileptonic tagging method, *Phys. Rev. Lett.* **124**, 161803 (2020).
- [22] Belle Collaboration, Measurement of the  $\tau$  lepton polarization and  $R(D^*)$  in the decay  $\bar{B} \rightarrow D^*\tau^{-}\bar{\nu}_{\tau}$  with one-prong hadronic  $\tau$  decays at Belle, *Phys. Rev. D* **97**, 012004 (2018).
- [23] Belle Collaboration, Measurement of the branching ratio of  $\bar{B}^0 \rightarrow D^{*+}\tau^{-}\bar{\nu}_{\tau}$  relative to  $\bar{B}^0 \rightarrow D^{*+}\ell^{-}\bar{\nu}_{\ell}$  decays with a semileptonic tagging method, *Phys. Rev. D* **94**, 072007 (2016).
- [24] Belle Collaboration, Measurement of the  $\tau$  Lepton Polarization and  $R(D^*)$  in the Decay  $\bar{B} \rightarrow D^*\tau^{-}\bar{\nu}_{\tau}$ , *Phys. Rev. Lett.* **118**, 211801 (2017).
- [25] Belle Collaboration, Measurement of the branching ratio of  $\bar{B} \rightarrow D^{(*)}\tau^{-}\bar{\nu}_{\tau}$  relative to  $\bar{B} \rightarrow D^{(*)}\ell^{-}\bar{\nu}_{\ell}$  decays with hadronic tagging at Belle, *Phys. Rev. D* **92**, 072014 (2015).
- [26] LHCb Collaboration, Measurement of the Ratio of the  $B^0 \rightarrow D^{*-}\tau^{+}\nu_{\tau}$  and  $B^0 \rightarrow D^{*-}\mu^{+}\nu_{\mu}$  Branching Fractions Using Three-Prong  $\tau$ -lepton Decays, *Phys. Rev. Lett.* **120**, 171802 (2018).
- [27] LHCb Collaboration, Measurement of the Ratio of Branching Fractions  $\mathcal{B}(B^0 \rightarrow D^{*+}\tau^{-}\bar{\nu}_{\tau})/\mathcal{B}(B^0 \rightarrow D^{*+}\mu^{-}\bar{\nu}_{\mu})$ , *Phys. Rev. Lett.* **115**, 111803 (2015); **115**, 159901(E) (2015).
- [28] David Marzocca, Ui Min, and Minho Son, Bottom-flavored mono-tau tails at the LHC, *J. High Energy Phys.* **12** (2020) 035.
- [29] Motoi Endo, Syuhei Iguro, Teppei Kitahara, Michihisa Takeuchi, and Ryountaro Watanabe, Non-resonant new physics search at the LHC for the  $b \rightarrow c\tau\nu$  anomalies, *J. High Energy Phys.* **02** (2022) 106.
- [30] John D. Gómez, Néstor Quintero, and Eduardo Rojas, Charged current  $b \rightarrow c\tau\bar{\nu}_{\tau}$  anomalies in a general  $W'$  boson scenario, *Phys. Rev. D* **100**, 093003 (2019).
- [31] Syuhei Iguro, Michihisa Takeuchi, and Ryountaro Watanabe, Testing leptoquark/EFT in  $\bar{B} \rightarrow D^{(*)}l\bar{\nu}$  at the LHC, *Eur. Phys. J. C* **81**, 406 (2021).
- [32] Syuhei Iguro, Yuji Omura, and Michihisa Takeuchi, Test of the  $R(D^{(*)})$  anomaly at the LHC, *Phys. Rev. D* **99**, 075013 (2019).
- [33] Mohammad Abdullah, Julian Calle, Bhaskar Dutta, Andres Florez, and Diego Restrepo, Probing a simplified  $w'$  model of  $r_{D^{(*)}}$  anomalies using  $b$  tags,  $\tau$  leptons, and missing energy, *Phys. Rev. D* **98**, 055016 (2018).
- [34] Wolfgang Altmannshofer, P. S. Bhupal Dev, and Amarjit Soni,  $R_{D^{(*)}}$  anomaly: A possible hint for natural supersymmetry with  $R$ -parity violation, *Phys. Rev. D* **96**, 095010 (2017).
- [35] V. Barger, Wai-Yee Keung, and Ernest Ma, Sequential  $w$  and  $z$  bosons, *Phys. Lett.* **94B**, 377 (1980).
- [36] Jack Y. Araz, Mariana Frank, Benjamin Fuks, Stefano Moretti, and Özer Özdal, Cross-fertilising extra gauge boson searches at the LHC, *J. High Energy Phys.* **11** (2021) 014.
- [37] Andrés Flórez, Alfredo Gurrola, Will Johns, Young Do Oh, Paul Sheldon, Dylan Teague, and Thomas Weiler, Searching for new heavy neutral gauge bosons using vector boson fusion processes at the LHC, *Phys. Lett. B* **767**, 126 (2017).
- [38] Andrey Grozin, Effective field theories, *Particles* **3**, 245 (2020).
- [39] A. V. Manohar, Effective field theories, *Lect. Notes Phys.* **479**, 311 (1997).
- [40] Aneesh V. Manohar, Introduction to effective field theories, arXiv:1804.05863.
- [41] Ilaria Brivio and Michael Trott, The standard model as an effective field theory, *Phys. Rep.* **793**, 1 (2019).
- [42] W. Buchmuller and D. Wyler, Effective Lagrangian analysis of new interactions and flavor conservation, *Nucl. Phys.* **B268**, 621 (1986).
- [43] Adam Falkowski, Martín González-Alonso, and Kin Mimouni, Compilation of low-energy constraints on 4-fermion operators in the SMEFT, *J. High Energy Phys.* **08** (2017) 123.
- [44] Admir Greljo, Jorge Martin Camalich, and José David Ruiz-Álvarez, Mono- $\tau$  Signatures at the LHC Constrain Explanations of  $B$ -decay Anomalies, *Phys. Rev. Lett.* **122**, 131803 (2019).

- [45] J. Alwall, R. Frederix, S. Frixione, V. Hirschi, F. Maltoni, O. Mattelaer, H. S. Shao, T. Stelzer, P. Torrielli, and M. Zaro, The automated computation of tree-level and next-to-leading order differential cross sections, and their matching to parton shower simulations, *J. High Energy Phys.* **07** (2014) 079.
- [46] Richard D. Ball *et al.*, Parton distributions for the LHC Run II, *J. High Energy Phys.* **04** (2015) 040.
- [47] Torbjörn Sjöstrand, Stefan Ask, Jesper R. Christiansen, Richard Corke, Nishita Desai, Philip Ilten, Stephen Mrenna, Stefan Prestel, Christine O. Rasmussen, and Peter Z. Skands, An introduction to PYTHIA 8.2, *Comput. Phys. Commun.* **191**, 159 (2015).
- [48] J. de Favereau, C. Delaere, P. Demin, A. Giammanco, V. Lemaitre, A. Mertens, and M. Selvaggi, DELPHES 3, A modular framework for fast simulation of a generic collider experiment, *J. High Energy Phys.* **02** (2014) 057.
- [49] Johan Alwall *et al.*, Comparative study of various algorithms for the merging of parton showers and matrix elements in hadronic collisions, *Eur. Phys. J. C* **53**, 473 (2008).
- [50] M. L. Mangano, M. Moretti, F. Piccinini, and M. Treccani, Matching matrix elements and shower evolution for top-quark production in hadronic collisions, *J. High Energy Phys.* **01** (2007) 013.
- [51] Adam Alloul, Neil D. Christensen, Céline Degrande, Claude Duhr, and Benjamin Fuks, FeynRules 2.0—A complete toolbox for tree-level phenomenology, *Comput. Phys. Commun.* **185**, 2250 (2014).
- [52] Celine Degrande, Claude Duhr, Benjamin Fuks, David Grellscheid, Olivier Mattelaer, and Thomas Reiter, UFO—The universal FeynRules output, *Comput. Phys. Commun.* **183**, 1201 (2012).
- [53] Lorenzo Moneta, K. Cranmer, G. Schott, and W. Verkerke, The RooStats project, *Proc. Sci. ACAT2010* (**2011**) 057.
- [54] Andrés Flórez, Alfredo Gurrola, Will Johns, Paul Sheldon, Elijah Sheridan, Kuver Sinha, and Brandon Soubasis, Probing axionlike particles with  $\gamma\gamma$  final states from vector boson fusion processes at the LHC, *Phys. Rev. D* **103**, 095001 (2021).
- [55] Andrés Flórez, Alfredo Gurrola, Will Johns, Jessica Maruri, Paul Sheldon, Kuver Sinha, and Savanna Rae Starko, Anapole dark matter via vector boson fusion processes at the LHC, *Phys. Rev. D* **100**, 016017 (2019).
- [56] Andrés Flórez, Yuhan Guo, Alfredo Gurrola, Will Johns, Oishik Ray, Paul Sheldon, and Savanna Starko, Probing heavy spin-2 bosons with  $\gamma\gamma$  final states from vector boson fusion processes at the LHC, *Phys. Rev. D* **99**, 035034 (2019).
- [57] Andrés Flórez, Kaiwen Gui, Alfredo Gurrola, Carlos Patiño, and Diego Restrepo, Expanding the reach of heavy neutrino searches at the LHC, *Phys. Lett. B* **778**, 94 (2018).
- [58] Andres Florez, Alfredo Gurrola, Will Johns, Young Do Oh, Paul Shendon, Dylan Teague, and Thomas Weiler, Searching for new heavy neutral gauge bosons using vector boson fusion processes at the LHC, *Phys. Lett. B* **767**, 126 (2017).
- [59] Andrés Flórez, Luis Bravo, Alfredo Gurrola, Carlos Ávila, Manuel Segura, Paul Sheldon, and Will Johns, Probing the stau-neutralino coannihilation region at the LHC with a soft tau lepton and a jet from initial state radiation, *Phys. Rev. D* **94**, 073007 (2016).
- [60] Jon Butterworth *et al.*, PDF4LHC recommendations for LHC Run II, *J. Phys. G* **43**, 023001 (2016).
- [61] A. M. Sirunyan *et al.*, Identification of heavy-flavour jets with the CMS detector in pp collisions at 13 TeV, *J. Instrum.* **13**, P05011 (2018).
- [62] Claudia Cornella, Darius A. Faroughy, Javier Fuentes-Martin, Gino Isidori, and Matthias Neubert, Reading the footprints of the B-meson flavor anomalies, *J. High Energy Phys.* **08** (2021) 050.
- [63] CMS Collaboration, Search for new physics in the tau plus missing transverse momentum final state in proton-proton collisions at  $\sqrt{s} = 13$  TeV, Technical Report No. CMS-EXO-21-009, CERN-EP-2022-268, CERN, Geneva, 2022.
- [64] Morad Aaboud *et al.*, Search for High-Mass Resonances Decaying to  $\tau\nu$  in pp Collisions at  $\sqrt{s} = 13$  TeV with the ATLAS Detector, *Phys. Rev. Lett.* **120**, 161802 (2018).
- [65] The search for a third-generation leptoquark coupling to a  $\tau$  lepton and a b quark through single, pair and nonresonant production at  $\sqrt{s} = 13$  TeV, Technical Report No. CMS-PAS-EXO-19-016, CERN, Geneva, 2022.